

Supplement of Weather Clim. Dynam., 5, 1207–1222, 2024
<https://doi.org/10.5194/wcd-5-1207-2024-supplement>
© Author(s) 2024. CC BY 4.0 License.



Supplement of

Impact of stochastic physics on the representation of atmospheric blocking in EC-Earth3

Michele Filippucci et al.

Correspondence to: Michele Filippucci (michele.filippucci@unitn.it)

The copyright of individual parts of the supplement might differ from the article licence.

1 The dependence of the climatological blocking frequency on model resolution

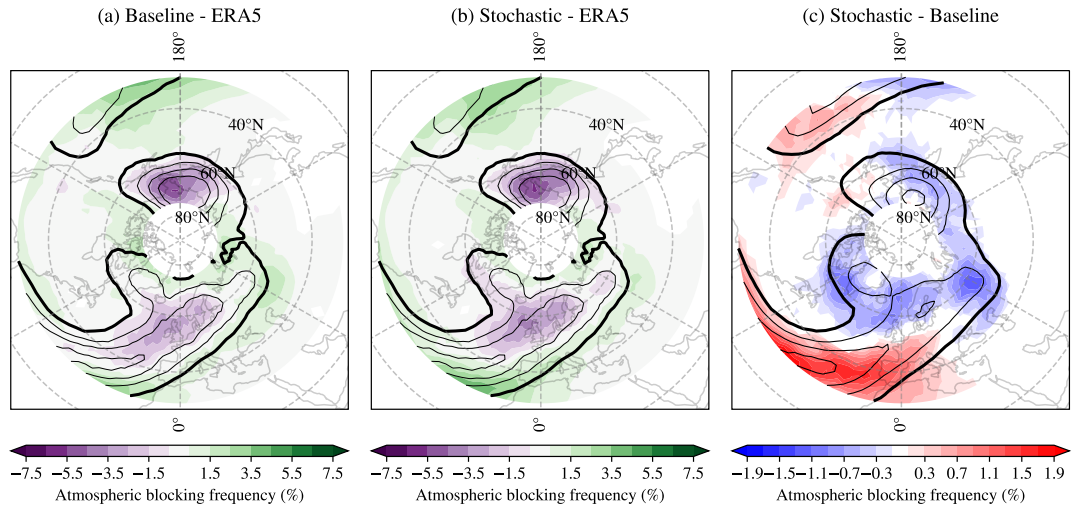


Figure S1: Climatological blocking frequency for December, January, February and March (DJFM) for TL159 (~ 125 km) model resolution given as percentage of blocked days: a) difference between the baseline version of the model and ERA5; b) difference between the stochastic version of the model and ERA5; c) difference between the stochastic and baseline versions of the model. In panels a) and b), shading shows differences in atmospheric blocking frequency, while black contours indicate blocking frequency in ERA5. In c), shading shows the difference in blocking frequency between the two model versions, while the black contours show blocking frequency from baseline ensemble. The thick contour refers to a frequency of 3% of days and contours are plotted every 3%

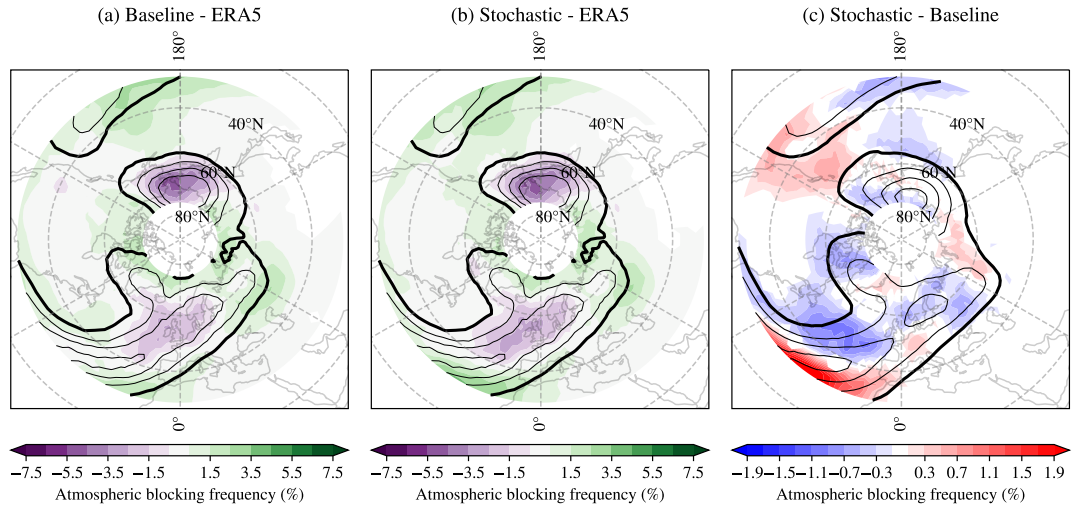


Figure S2: Climatological blocking frequency for December, January, February and March (DJFM) for TL255 (~ 80 km) model resolution. Plot description as in Figure S1.

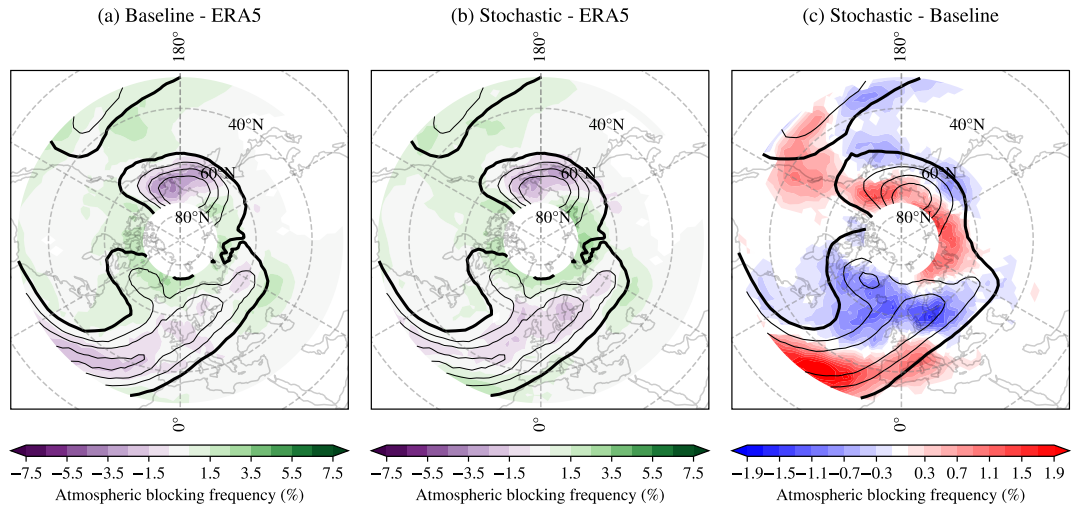


Figure S3: Climatological blocking frequency for December, January, February and March (DJFM) for TL511 (~ 40 km) model resolution. Plot description as in Figure S1.

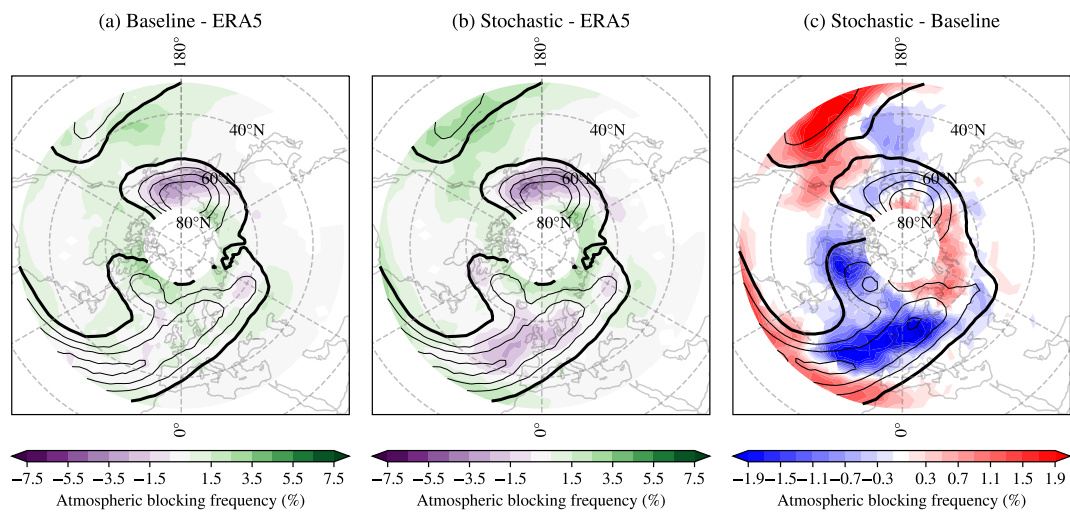


Figure S4: Climatological blocking frequency for December, January, February and March (DJFM) for TL799 (~ 25 km) model resolution. Plot description as in Figure S1.

2 Zonal wind in the meridional plane over the Atlantic sector

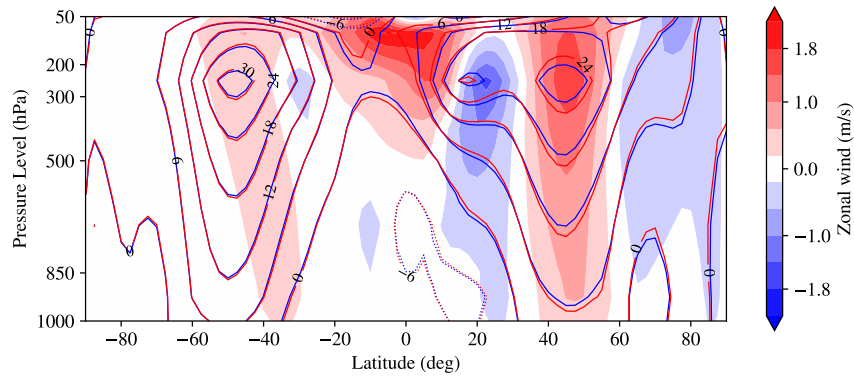


Figure S5: Zonal wind [$\frac{m}{s}$] averaged over the Atlantic sector (65W,5W). Red (blue) contours indicate the stochastic (baseline) ensemble average, while shading represents the difference between the stochastic and baseline runs.

3 Top of the atmosphere radiative budget

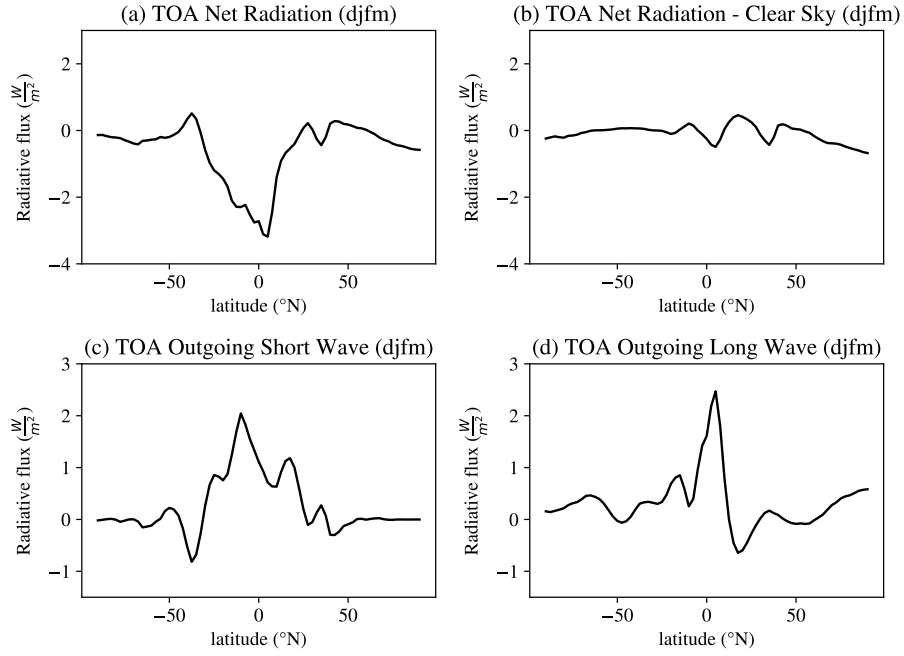
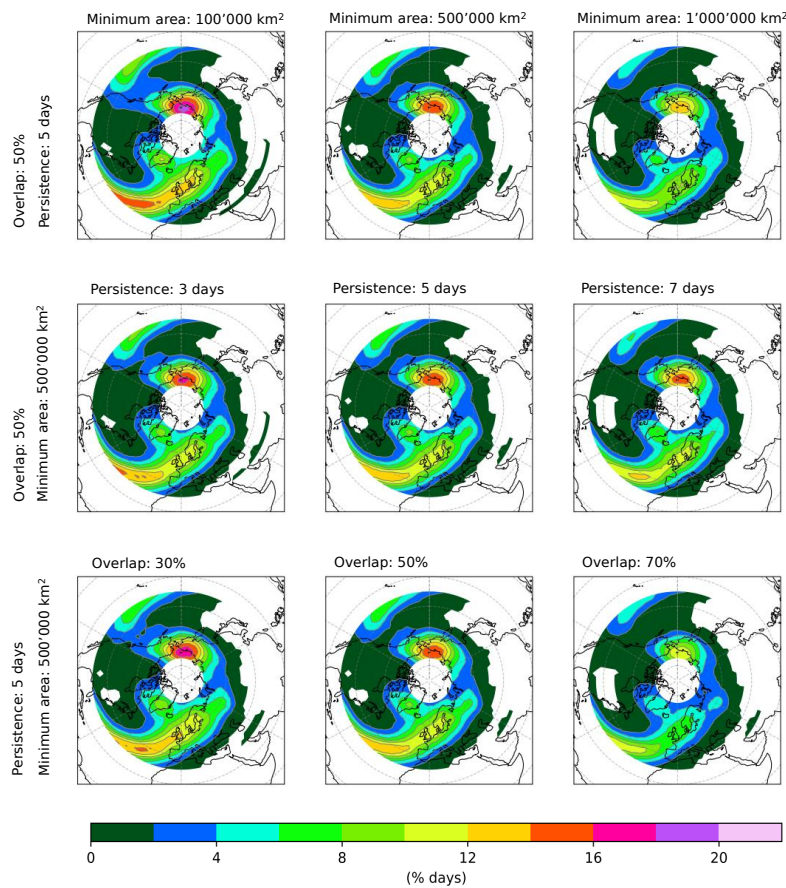


Figure S6: Differences in top-of-atmosphere (TOA) radiative fluxes [$\frac{W}{m^2}$] between the stochastic and baseline runs for the following quantities: a) TOA net radiative fluxes (Incoming shortwave - Outgoing shortwave - Outgoing longwave); b) Clear-sky TOA net radiative fluxes; c) TOA net shortwave radiation; d) TOA outgoing longwave radiation.

4 Impact of the chosen thresholds on the Lagrangian tracking algorithm for blocking detection

Figure S7: Climatological winter (djfm) atmospheric blocking frequency computed over ERA5 dataset 1979/2019. The frequency is given as percentage of blocked days and it has been calculated through the Lagrangian Tracking Algorithm based on the geopotential height gradient reversal index. Every plot corresponds to a set of chosen thresholds.



5 Climatological blocking frequency assessed through an anomaly based index for blocking detection

5.1 The GHA algorithm

We implemented a simple version of a Geopotential Height Anomaly (GHA) index based on Woollings et al. 2018. The algorithm works as follows:

- The daily geopotential height at 500hPa is used as input data. We use a grid of $2.5^\circ\text{lat} \times 2.5^\circ\text{lon}$ and we select the extended winter months (DJFM).
- We compute the daily geopotential height anomaly (Z') for each grid point of the input data. This is done by comparing the value of the geopotential height at each day and grid point with its mean value over a 90 days time window centered on the same day.
- We compute the standard deviation of the geopotential height anomaly over a longitude-latitude box $[180^\circ\text{W}, 180^\circ\text{E}]$, $[40^\circ\text{N}, 80^\circ\text{N}]$.
- We then identify the grid points where $Z' > M\sigma$. We set M to 1.26 in order to select values outside the 90% percentile of a normal distribution.
- Ultimately, we apply the Lagrangian tracking algorithm applying a persistence filter of 5 *days* and a minimum area filter of $2 \cdot 10^6 \text{ km}^2$. The chosen thresholds are coherent with what we found in Woollings et al. 2018.

5.2 Results discussion

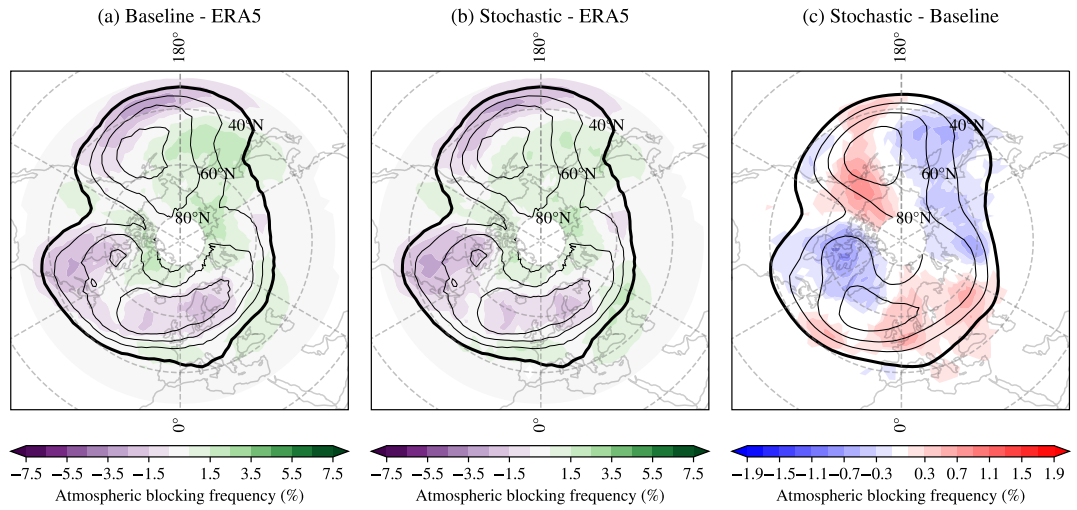
Figure S8a shows EC-Earth atmospheric blocking frequency assessed through the GHA index described above. The baseline version of EC-Earth underestimates blocking in the North Atlantic, except from higher latitudes, where blocking frequency seems to be slightly overestimated. Similarly, blocking frequency is underestimated in the Pacific at low latitudes and overestimated at high latitudes.

Moving to Figure S8b is possible to observe how stochastic parameterizations have a little impact on blocking representation, with small improvements observed in eastern Siberia and over the Bering strait.

Changes introduced by the stochastic parameterizations are more clearly shown in Figure S8c, where it is possible to see how stochastic parameterization are displacing atmospheric blocking climatological frequency eastward.

The changes depicted by the GHA index differ from the ones assessed through the gradient reversal (GR) index in the main text. While the latter shows a deterioration of blocking representation over Europe, the former shows a slight improvement when stochastic parameterizations are implemented over the Pacific and no notable change in the Atlantic. However, the changes observed through the GHA index are again coherent with our mean state analysis as the frequency maxima displacement can be again attributed to a more vigorous and zonal jet stream that displaces the Northern Hemisphere stationary waves crests and blocking further east. The two indices detect features of the flow that, despite having different characteristics, still meet the definition of blocking. The GHA index is able to identify geopotential height anomalies, including persistent ridges, while the GR index looks for wind reversal and breaking Rossby waves (Woollings et al. 2018). Hence, the results depicted here and in the main paper are not in contrast. Moreover, the fact that the differences depicted by the GR index are larger than those depicted by the GHA index highlights how the former is more sensitive to mean state changes, a fact that was already noted in an earlier study by Scaife et al. 2010.

Figure S8: Ensemble mean DJFM climatology (1979-2008) of atmospheric blocking frequency given as percentage of blocked days computed through an anomaly based index (GHA): a) difference between the baseline version of the model and ERA5; b) difference between the stochastic version of the model and ERA5; c) difference between the stochastic and baseline versions of the model. In panels a) and b), shading shows differences in atmospheric blocking frequency, while black contours indicate blocking frequency in ERA5. In c), shading shows the difference in blocking frequency between the two model versions, while the black contours show blocking frequency from baseline. The thick contour refers to a frequency of 3% of days and contours are plotted every 3%.



6 Comparison between the stochastic and baseline versions of the model and ERA5

Figure S9: DJFM Transient kinetic energy (TKE [$m^2 s^{-2}$]) at 250 hPa computed for the baseline version of EC-Earth model and ERA5 reanalysis. The black contours represent reanalysis, while shading shows the difference between the baseline simulations and reanalysis.

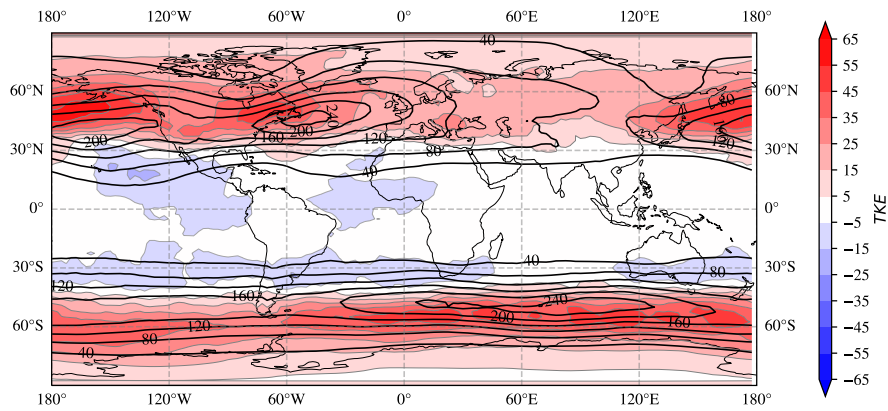


Figure S10: DJFM Transient kinetic energy (TKE [$m^2 s^{-2}$]) at 250 hPa computed for the stochastic version of EC-Earth model and ERA5 reanalysis. The black contours represent reanalysis, while shading shows the difference between the stochastic simulations and reanalysis.

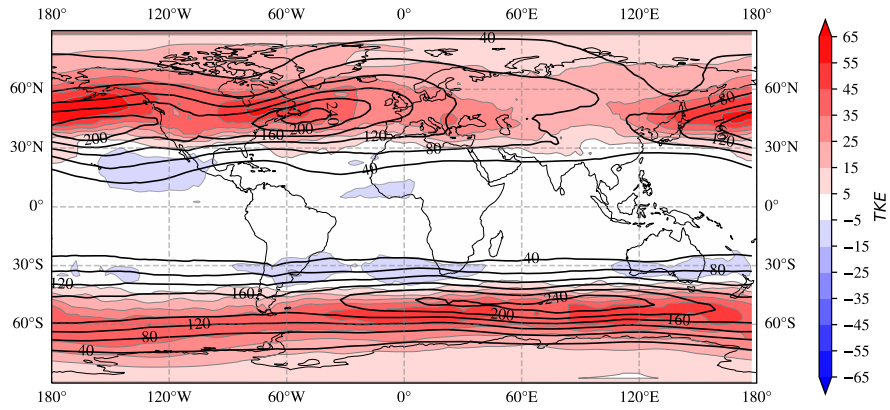


Figure S11: DJFM Eady growth rate (EGR, $[\text{day}^{-1}]$) at 850 hPa computed for the baseline version of EC-Earth model and ERA5 reanalysis. The black contours represent reanalysis, while shading shows the difference between the baseline simulations and reanalysis.

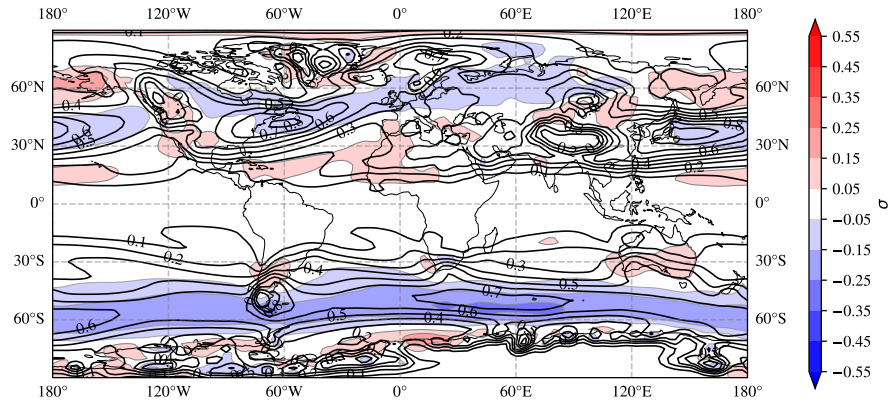
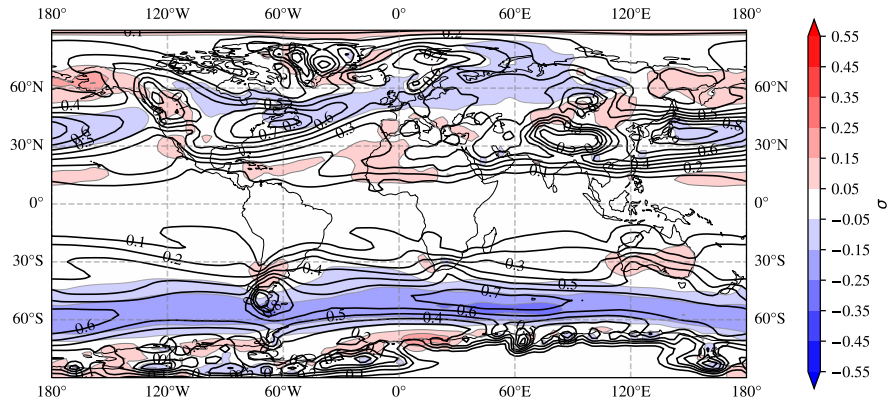


Figure S12: DJFM Eady growth rate (EGR, $[\text{day}^{-1}]$) at 850 hPa computed for the stochastic version of EC-Earth model and ERA5 reanalysis. The black contours represent reanalysis, while shading shows the difference between the stochastic simulations and reanalysis.



References

- Scaife, Adam A et al. (2010). “Atmospheric blocking and mean biases in climate models”. In: *Journal of Climate* 23.23, pp. 6143–6152.
- Woollings, Tim et al. (2018). “Blocking and its response to climate change”. In: *Current climate change reports* 4, pp. 287–300.